

# Van der Waals-coupled electronic states in incommensurate double-walled carbon nanotubes

Kaihui Liu<sup>\*1</sup>, Chenhao Jin<sup>\*1</sup>, Xiaoping Hong<sup>1</sup>, Jihoon Kim<sup>1</sup>, Alex Zettl<sup>1,2</sup>, Enge Wang<sup>3</sup>, Feng Wang<sup>1,2</sup>

**S1. Simulated absorption spectra of SWNT (22,9), (11,11) and (22,9)+(11,11)**

**S2. Theory of intertube electronic coupling**

**S3. Requirement for strong intertube electronic coupling**

**S4.  $1/\Delta E_{i\beta}$  pattern for different nanotube diameters and transitions**

**S5. Electron diffraction pattern for all 28 DWNTs**

**S6. Optical transition data Table for all 28 DWNTs**

### S1. Simulated absorption spectra of SWNT (22,9), (11,11) and (22,9)+(11,11)

The optical absorption spectra of individual single-walled nanotube were simulated based on Ref. 1-3. If there is no inter-tube coupling, the absorption of double-walled nanotubes will be the sum of the constituent single-walled nanotube absorption (Fig. S1). The shape of observed DWNT (22,9)/(11,11) absorption spectrum (Fig. 1c) is very similar to the simulated one, except that all the transition peaks are shifted in energy due to tube-tube interactions.

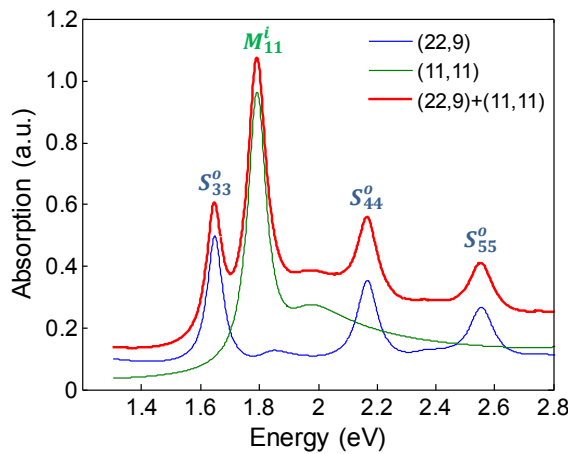


Figure S1. Simulated absorption spectrum of SWNT (22,9), (11,11) and their sum.

### S2. Theory of intertube electronic couplings

To calculate the intertube electronic coupling, we consider an electronic state  $\alpha(\mu, k, \sigma)$  in one constituent SWNT -- without loss of generality, we assume it to be the inner tube -- and treat its interaction with the outer tube as a perturbation. From second order perturbation theory, the eigenenergy of  $\alpha(\mu, k, \sigma)$  is:

$$E_\alpha = E_\alpha^0 + \delta E_\alpha^{el} = E_\alpha^0 + \sum_{\beta} \frac{|M_{\alpha\beta}|^2}{E_\alpha^0 - E_\beta^0}, \quad (S1)$$

where  $\beta(\mu', k', \sigma')$  labels electronic states of outer tube and the sum goes over all the outer tube states. Each state  $\alpha$ ,  $\beta$  corresponds to a specific wavevector in the 2D graphene

Brillouin zone using the zone-folding scheme. The matrix element  $M_{\alpha\beta} = \langle \Psi_\alpha | H_{INT} | \Psi_\beta \rangle$

describes the coupling between inner tube state  $\alpha$  and outer tube state  $\beta$ .  $\Psi_\alpha$ ,  $\Psi_\beta$  are electronic wavefunctions of unperturbed SWNTs, thus in a  $\pi$ -orbit tight-binding model can be explicitly written as:

$$|\Psi_\alpha\rangle = \frac{1}{\sqrt{2N}} \sum_{\mathbf{R}_j} e^{i(\mu\theta_j + kz_j)} (|\mathbf{r} - \mathbf{R}_j\rangle + \sigma e^{i\phi_\alpha} |\mathbf{r} - \mathbf{R}_j - \boldsymbol{\tau}\rangle) = |\Psi_{\mu k}^A\rangle + \sigma |\Psi_{\mu k}^B\rangle. \quad (\text{S2})$$

Here  $\mathbf{R}_j = (\theta_j, z_j)$  is the coordinate of a graphene unit cell on the nanotube, which is summed over all unit cells (with N being the total number);  $\boldsymbol{\tau}$  is the vector connecting sublattice A and B in a graphene unit cell;  $\phi_\alpha$  is the phase difference between two sublattices. Then we can expand  $M_{\alpha\beta}$  as  $M_{\alpha\beta}^{AA} + \sigma' M_{\alpha\beta}^{AB} + \sigma M_{\alpha\beta}^{BA} + \sigma\sigma' M_{\alpha\beta}^{BB}$ , each representing the interaction between one sublattice of inner tube and one sublattice of outer tube atoms, with

$$\begin{aligned} M_{\alpha\beta}^{AA} &= \frac{1}{2\sqrt{NN'}} \sum_{\mathbf{R}_j} e^{i[(\mu' - \mu)\theta_j + (k' - k)z_j]} \sum_{\mathbf{R}'_i} e^{i[\mu'\Delta\theta + k'\Delta z]} t(\Delta\mathbf{R}) \\ M_{\alpha\beta}^{AB} &= \frac{1}{2\sqrt{NN'}} e^{i\phi_\beta} \sum_{\mathbf{R}_j} e^{i[(\mu' - \mu)\theta_j + (k' - k)z_j]} \sum_{\mathbf{R}'_i} e^{i[\mu'\Delta\theta + k'\Delta z]} t(\Delta\mathbf{R} + \boldsymbol{\tau}') \\ M_{\alpha\beta}^{BA} &= \frac{1}{2\sqrt{NN'}} e^{-i\phi_\alpha} \sum_{\mathbf{R}_j} e^{i[(\mu' - \mu)\theta_j + (k' - k)z_j]} \sum_{\mathbf{R}'_i} e^{i[\mu'\Delta\theta + k'\Delta z]} t(\Delta\mathbf{R} - \boldsymbol{\tau}) \\ M_{\alpha\beta}^{BB} &= \frac{1}{2\sqrt{NN'}} e^{i(\phi_\beta - \phi_\alpha)} \sum_{\mathbf{R}_j} e^{i[(\mu' - \mu)\theta_j + (k' - k)z_j]} \sum_{\mathbf{R}'_i} e^{i[\mu'\Delta\theta + k'\Delta z]} t(\Delta\mathbf{R} + \boldsymbol{\tau}' - \boldsymbol{\tau}), \end{aligned} \quad (\text{S3})$$

in which  $\Delta\mathbf{R} = \mathbf{R}'_i - \mathbf{R}_j = (\Delta\theta, \Delta z)$  is the coordinate difference between an inner tube atom at  $\mathbf{R}_j$  and an outer tube atom at  $\mathbf{R}'_i$ , whose interaction is described by  $t(\Delta\mathbf{R})$ .

Due to the incommensurate inner/outer tube lattice, we can assume that outer wall atoms are distributing randomly around any given inner-wall atom and approximate the sum over  $\mathbf{R}'_i$  with an integral over outer tube surface:

$$\sum_{\mathbf{R}'_i} e^{i[\mu' \Delta\theta + k' \Delta z]} t(\Delta\theta, \Delta z) = \frac{1}{S_0} \iint_{\text{outertube}} r_o d\theta dz e^{i[\mu' \Delta\theta + k' \Delta z]} t(\theta, z) \quad (\text{S4})$$

which is simply the Fourier component of pair interaction potential  $t(\theta, z)$  and is independent on  $\mathbf{R}_j$  ( $S_0$  is the graphene unit cell area).

### S3. Requirement for strong intertube electronic coupling

Here we use exponential decay form  $t(\Delta\theta, \Delta z) = \gamma e^{-r/\lambda} \approx \gamma e^{-\sqrt{\Delta r^2 + (\Delta r \Delta\theta)^2 + \Delta z^2}/\lambda}$  to describe the pair interaction, with the interatom distance  $r$ , the intertube spacing  $\Delta r$ , the interaction strength  $\gamma = 405 \gamma_0 \approx 1200$  eV and the characteristic length  $\lambda = 0.045$  nm (Ref. 4, 5).  $M_{\alpha\beta}^{AA}$  can then be calculated as:

$$M_{\alpha\beta}^{AA} = \delta_{\mathbf{q}+\mathbf{G}_i, \mathbf{q}'} \frac{2\pi\lambda\Delta r}{S_0} \gamma e^{-\Delta r/\lambda} e^{-\frac{\lambda\Delta r}{2}(k'^2 + \frac{\mu^2}{r_i r_o})}. \quad (\text{S5})$$

Where  $\mathbf{q} = \frac{\mu}{r_i} \hat{\theta} + k \hat{\mathbf{z}}$ ,  $\mathbf{q}' = \frac{\mu'}{r_o} \frac{r_o}{r_i} \hat{\theta} + k' \hat{\mathbf{z}} = \frac{\mu'}{r_o} \eta \hat{\theta} + k' \hat{\mathbf{z}}$ . Similar calculation can be done for  $M_{\alpha\beta}^{AB}$ ,

$M_{\alpha\beta}^{BA}$  and  $M_{\alpha\beta}^{BB}$  to give  $M_{\alpha\beta}$ :

$$M_{\alpha\beta} = C_{\alpha\beta} M_{\alpha\beta}^{AA}, \\ C_{\alpha\beta} = (1 + \sigma e^{-i\varphi_\alpha})(1 + \sigma' e^{i\varphi_\beta}), \quad \varphi_\alpha = \phi_\alpha - \mathbf{q} \cdot \boldsymbol{\tau}, \quad \varphi_\beta = \phi_\beta - \mathbf{q}' \cdot \boldsymbol{\tau}'. \quad (\text{S6})$$

The requirement for strong coupling is given by equation (S5). The Dirac delta function strictly requires  $\mathbf{q}' = \mathbf{q} + \mathbf{G}_i$ , corresponding to the solid dots in Fig. 3b. In addition, the term

$e^{-\frac{\lambda\Delta r}{2}(k'^2 + \frac{\mu^2}{r_i r_o})}$  indicates that the coupling decays very fast with large  $|\mathbf{q}'|$ . As a result, only the

three  $\mathbf{q}'$  (red dots in Fig. 3b) can couple strongly with the inner wall state at  $\mathbf{q}$ . Equation (S1) can then be written as:

$$\delta E_{\alpha}^{el} = \sum_{\beta=1}^3 \frac{|M_{\alpha\beta}|^2}{E_{\alpha}^0 - E_{\beta}^0}. \quad (S7)$$

In which we only need consider the coupling with three states (only  $\sigma = \sigma'$  case is included for small energy difference).

The transition energy shift for a given optical transition  $E_{ii}$  at wavevector  $(\mu, k)$  can be calculated as:

$$\begin{aligned} \delta E_{ii}^{el} &= \delta E_{\mu k+}^{el} - \delta E_{\mu k-}^{el} = \sum_{\beta=1}^3 \frac{|M_{\mu k+, \mu' k'_\beta +}|^2}{E_{\mu k+}^0 - E_{\mu' k'_\beta +}^0} - \sum_{\beta=1}^3 \frac{|M_{\mu k-, \mu' k'_\beta -}|^2}{E_{\mu k-}^0 - E_{\mu' k'_\beta -}^0} \\ &\approx \sum_{\beta=1}^3 \frac{|M_{\mu k+, \mu' k'_\beta +}|^2 + |M_{\mu k-, \mu' k'_\beta -}|^2}{E_{\mu k+}^0 - E_{\mu' k'_\beta +}^0} = \sum_{\beta=1}^3 \frac{|A_{i\beta}|^2}{\Delta E_{i\beta}} \end{aligned} \quad (S8)$$

where  $|A_{i\beta}|^2 = |M_{\mu k+, \mu' k' +}|^2 + |M_{\mu k-, \mu' k' -}|^2$  is the matrix element combining contribution from both valence and conduction band states;  $\Delta E_{i\beta} = E_{\mu k+}^0 - E_{\mu' k'_\beta +}^0$ . In the third step, we have introduced the approximation  $E_{\mu k+}^0 - E_{\mu' k'_\beta +}^0 \approx -(E_{\mu k-}^0 - E_{\mu' k'_\beta -}^0)$  due to the electron-hole symmetry for states close to the K and K' point.

#### S4. $1/\Delta E_{i\beta}$ Pattern for different nanotube diameters and transitions

Equation S8 shows that the energy shift  $\delta E_{ii}^{el}$  is determined by both matrix element  $M_{i\beta}$  and energy difference  $\Delta E_{i\beta}$ .  $M_{i\beta}$  has a simple form and is only sensitive to intertube spacing (Fig. 3c), therefore the rich behavior of energy shift origins largely from the  $\Delta E_{i\beta}$  term. Here we investigate in detail the pattern of  $1/\Delta E_{i\beta}$  for optical transitions of semiconducting inner-wall tubes. The results can be directly extended to metallic and outer-wall tubes.

The white contour line in Fig. 3d,e corresponds to the largest  $|1 / \Delta E_{i\beta}|$  (i.e. strongest electronic couplings), and it shows an interesting dependence on the inner and outer tube chiral angles for a given optical transition and inner-wall tube diameter. Here we study how this strong-coupling contour line evolves with different optical transitions (Fig. S2a) and with varying nanotube diameters (Fig. S2b).

In Fig. S2a we examine its dependence on different optical transitions for a fixed nanotube diameter ( $d_i=1\text{nm}$ ). The strong-coupling contour pattern line shrinks with decreasing transition index (or equivalently lower transition energy). It suggests that the probability to have strong inter-tube coupling becomes lower for low energy transitions.

Figure S2b shows the diameter dependence of the strong-coupling contour line for the  $S_{22}$  transition with  $d_i = 0.5, 1.0, 2.0\text{ nm}$ . The strong-coupling contour line pattern shrinks with increasing diameter, largely due to the lower transition energy of  $S_{22}$  for a larger diameter tube. Besides, we notice that for the large diameter limit, this contour line approaches to the requirement of  $\theta_{\text{twist}}=0$ . But for small diameter nanotubes, the contour pattern line rotates away from a line of constant twist angle. It shows that the electronic coupling in DWNT is not only determined by the inter-tube twist angle, but also the chiral angle of each tube. This feature comes from the unique “stretching” characteristic of the 1D bilayer system.

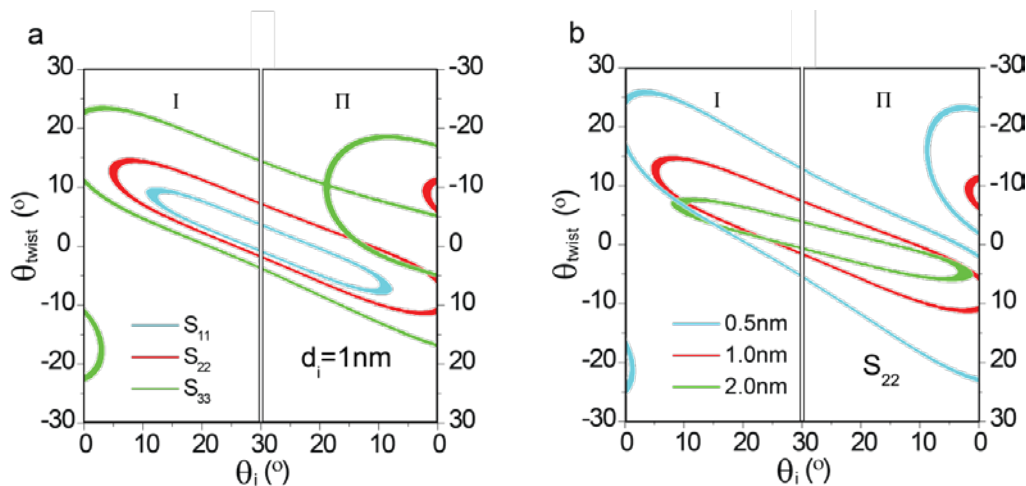
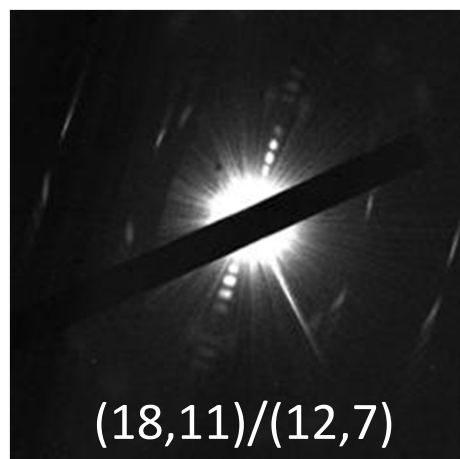
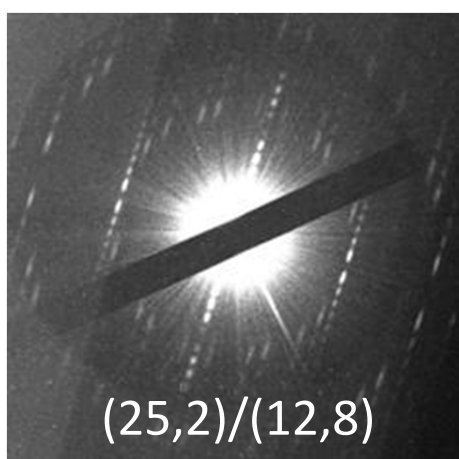
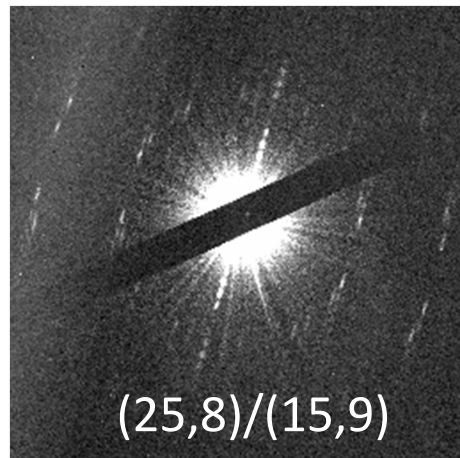
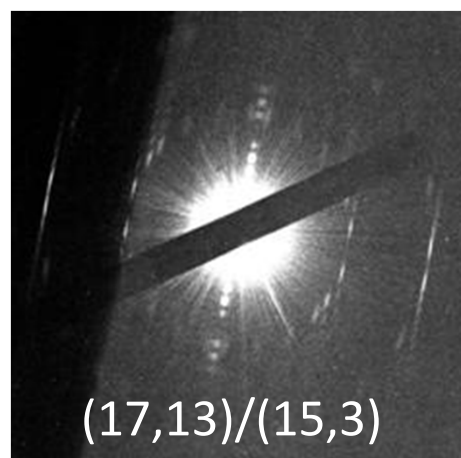
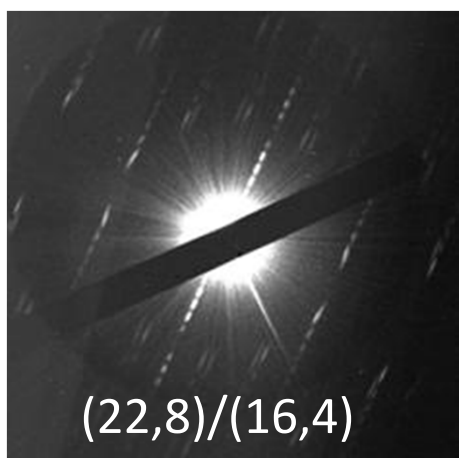
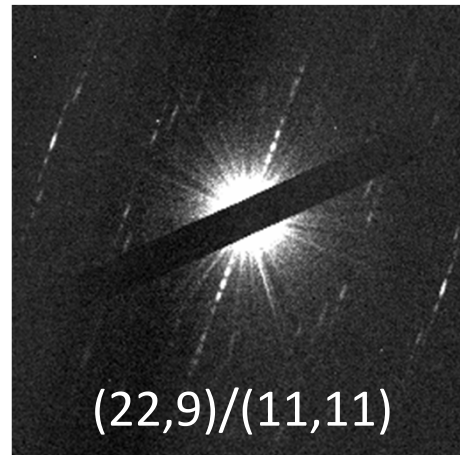
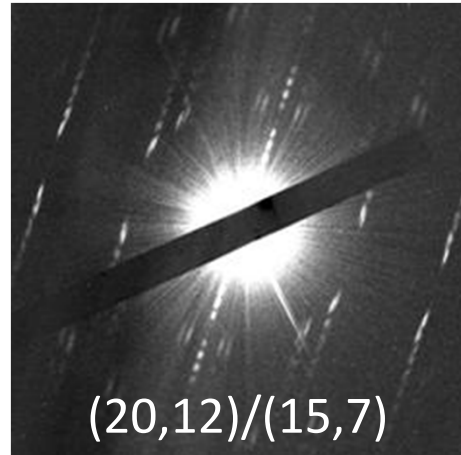
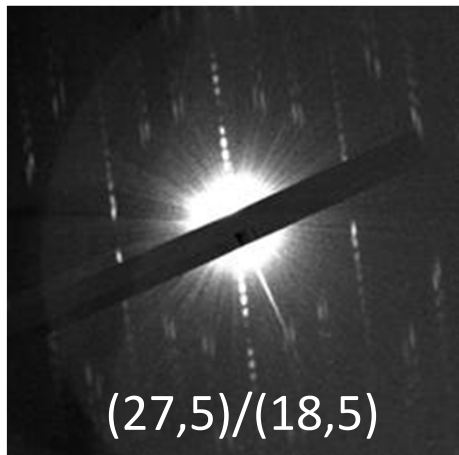
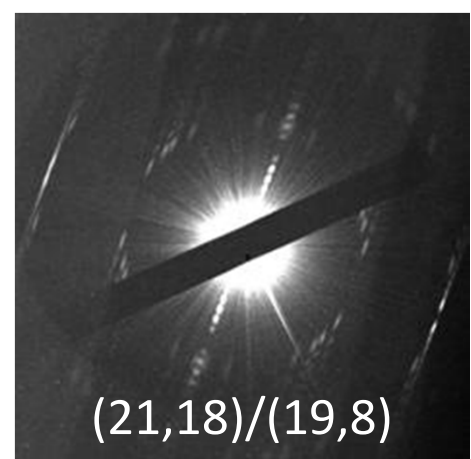
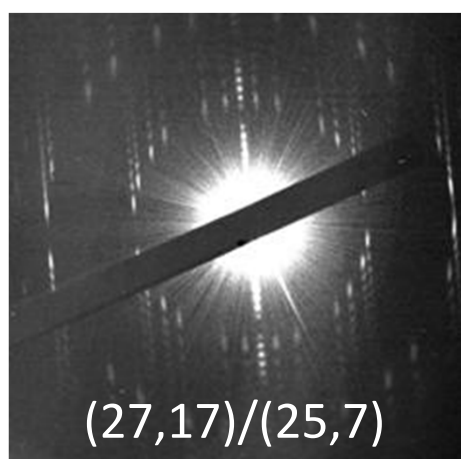
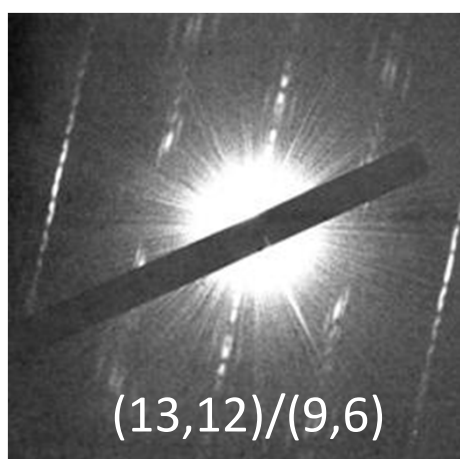
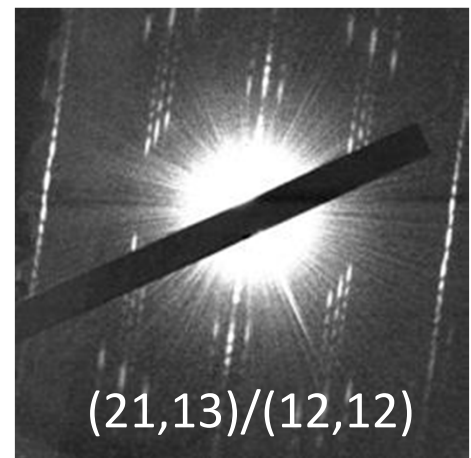
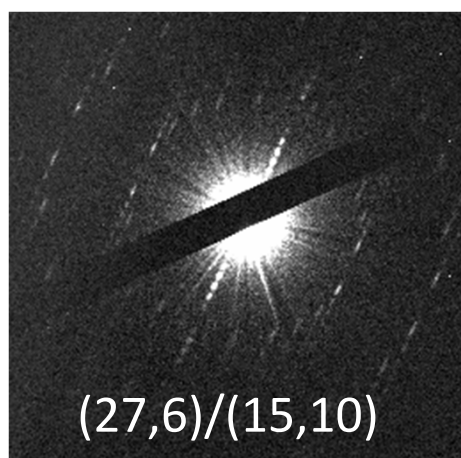
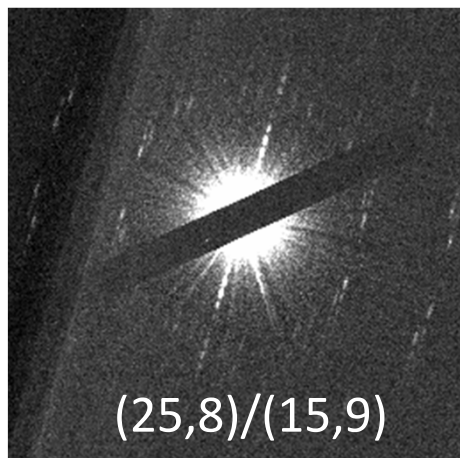
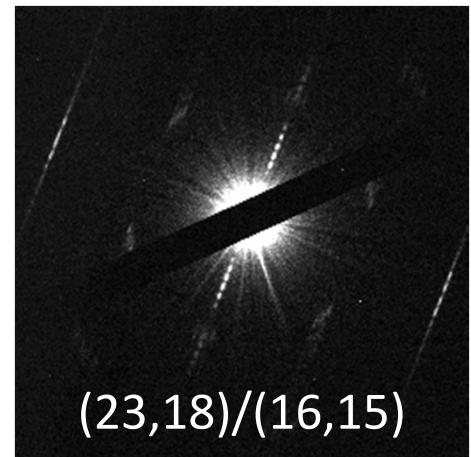
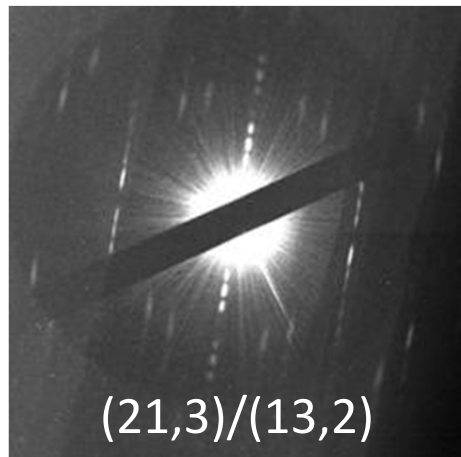
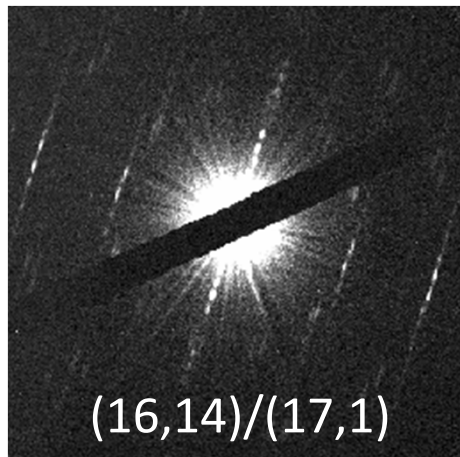


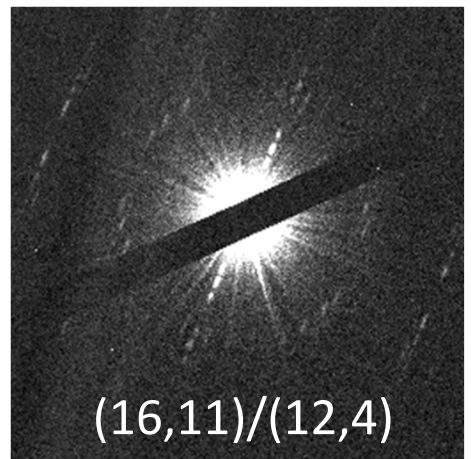
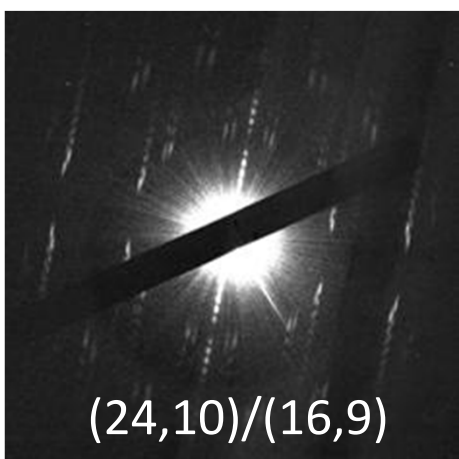
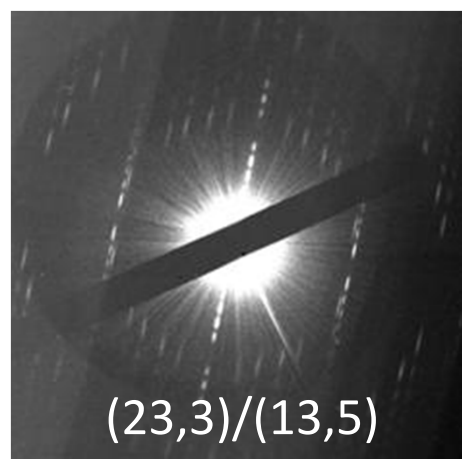
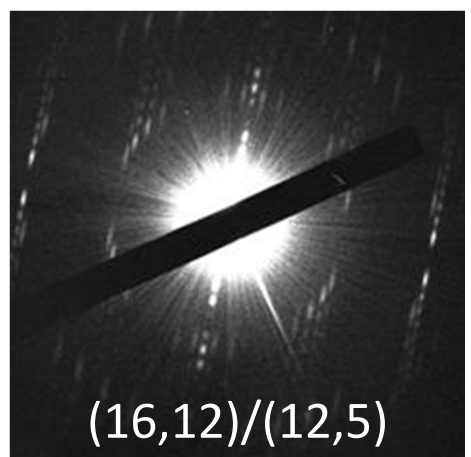
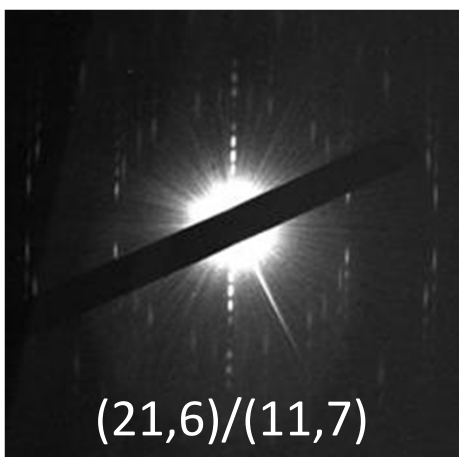
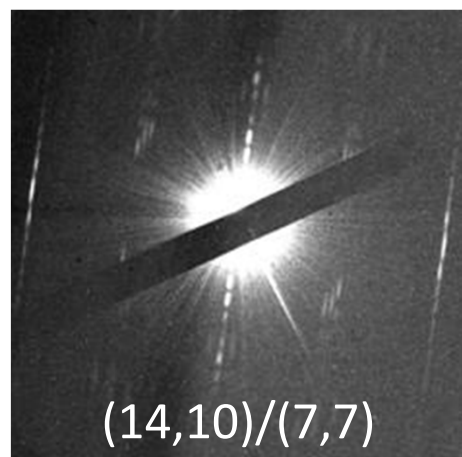
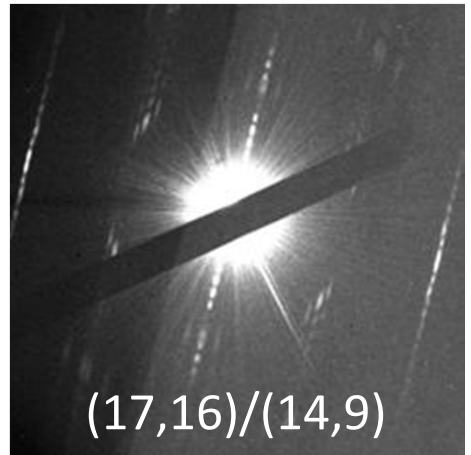
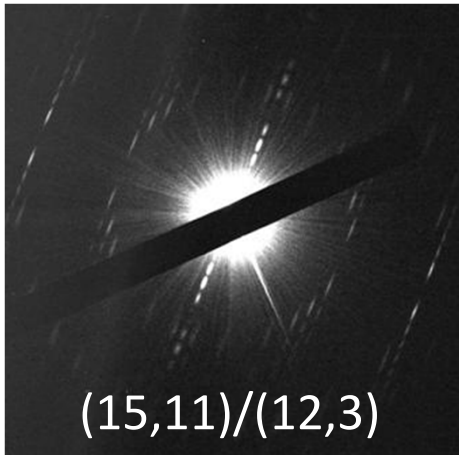
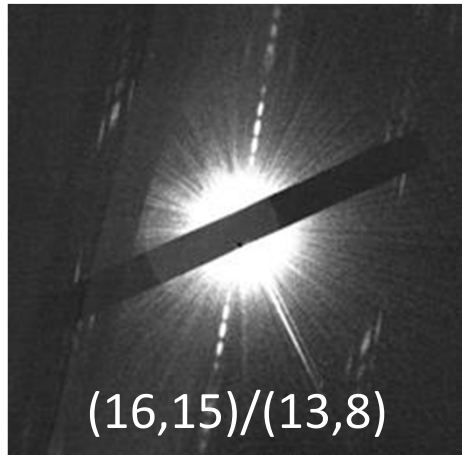
Figure S2. (a) Dependence of the strong-coupling contour line on transition energy with  $d_i = 1.0\text{ nm}$ . (b) Dependence of the strong-coupling contour line on inner-tube diameter  $d_i$  for  $S_{22}$  transition. The intertube spacing is fixed to 0.35 nm.

**References:**

- 1 Liu, K. *et al.* An atlas of carbon nanotube optical transitions. *Nature Nanotechnology* **7**, 325-329 (2012).
- 2 Choi, S., Deslippe, J., Capaz, R. B. & Louie, S. G. An Explicit Formula for Optical Oscillator Strength of Excitons in Semiconducting Single-Walled Carbon Nanotubes: Family Behavior. *Nano Letters* **13**, 54-58 (2013).
- 3 Liu, K. *et al.* Systematic Determination of Absolute Absorption Cross-section of Individual Carbon Nanotubes. *arXiv*, 1311.3328 (2013).
- 4 Saito, R., Dresselhaus, G. & Dresselhaus, M. S. Electronic-Structure of Double-Layer Graphene Tubules. *Journal of Applied Physics* **73**, 494-500 (1993).
- 5 Roche, S., Triozon, F., Rubio, A. & Mayou, D. Conduction mechanisms and magnetotransport in multiwalled carbon nanotubes. *Physical Review B* **64**, 121401 (2001).







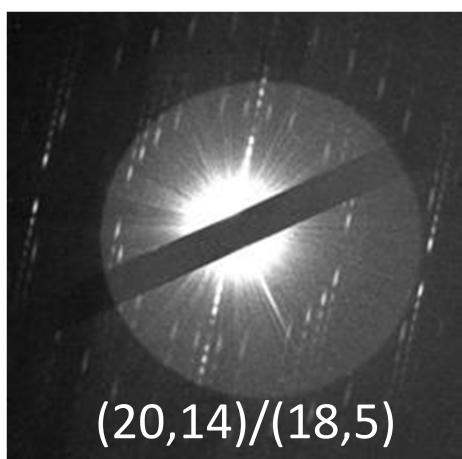
Supp

transi

is the

(s=-1)

or zig



(20,14)/(18,5)

**lementary Table S1.** Chiral indices and optical transition data for DWNT ( $n_o, m_o$ )/( $n_i, m_i$ ).  $E_{ii}^{DW}$  and  $E_{ii}^{SW}$  are the optical energies of nanotubes in DWNTs and as isolated SWNTs, respectively.  $\delta E^{\text{Exp}} = E_{ii}^{DW} - E_{ii}^{SW}$ ,  $\delta E^{\text{tot}} = \delta E^{\text{el}} - 55$ , where  $\delta E^{\text{el}}$  is the theoretical electronic coupling induced optical transition change; and 55 meV comes from the dielectric screening effects. The symbol  $\square$  indicates the inner and outer tubes have the same (opposite) handedness (left-handed or right-handed). If one wall is armchair and the other is zigzag the DWNT has no handedness, and  $s=0$ .

$m_i$	$n_o$	$m_o$	index	$E_{ii}^{DW}$ (eV)	$E_{ii}^{SW}$ (eV)	$\delta E^{\text{Exp}}$ (meV)	$s$	$\delta E^{\text{el}}$ (meV)	$\delta E^{\text{tot}}$ (meV)
8	5	27	$S_{33}^i$	1.905	2.03	-125	1	-40	-95
8	5	27	$S_{33}^o$	1.485	1.54	-55	1	-10	-65
8	5	27	$S_{44}^o$	2	2.06	-60	1	0	-55
8	5	27	$S_{55}^o$	2.38	2.4	-20	1	45	-10
5	3	17	$M_{11}^i$	1.74	1.82	-80	1	-25	-80
5	3	17	$M_{11}^i$	2.005	2.11	-105	1	-30	-85
5	3	17	$S_{33}^o$	1.695	1.78	-85	1	0	-55
5	3	17	$S_{44}^o$	2.08	2.21	-130	1	-50	-105
5	9	25	$M_{11}^i$	1.49	1.59	-100	1	-35	-90
5	9	25	$M_{11}^i$	1.605	1.67	-65	1	-30	-85
5	9	25	$S_{33}^o$	1.62	1.67	-50	1	0	-55
5	9	25	$S_{44}^o$	1.78	1.86	-80	1	-15	-70
8	3	19	$M_{11}^i$	1.495	1.61	-115	1	-25	-80
8	3	19	$M_{11}^i$	1.77	1.83	-60	1	-30	-85
8	3	19	$S_{33}^o$	1.61	1.69	-80	1	-5	-60
8	3	19	$S_{44}^o$	1.92	1.98	-60	1	0	-55

3	2	21	3	$S_{22}^i$	1.39	1.46	-70	1	-20		-75 1
3	2	21	3	$M_{11}^o$	1.41	1.46	-50	1	-5		-60 1
3	2	21	3	$M_{11}^o$	1.575	1.61	-35	1	0		-55 1
3	2	21	3	$M_{22}^o$	2.495	2.51	-15	1	20		-35 1
6	15	23	18	$S_{33}^i$	1.66	1.76	-100	1	-60		-1151
6	15	23	18	$S_{44}^i$	2.09	2.13	-40	1	0		-55 1
6	15	23	18	$S_{44}^o$	1.63	1.66	-30	1	50		-5 1
6	15	23	18	$S_{55}^o$	2.18	2.28	-100	1	-10		-65 1
5	9	25	8	$M_{11}^i$	1.5	1.59	-90	1	-35		-90 1
5	9	25	8	$M_{11}^i$	1.61	1.67	-60	1	-35		-90 1
5	9	25	8	$S_{33}^o$	1.61	1.67	-60	1	0		-55 1
5	9	25	8	$S_{44}^o$	1.79	1.86	-70	1	-15		-70 1
5	9	25	8	$S_{55}^o$	2.61	2.72	-110	1	-55		-1101
5	10	27	6	$S_{33}^i$	2.02	2.13	-110	1	-55		-1101
5	10	27	6	$S_{44}^i$	2.28	2.41	-130	1	-75		-1301
5	10	27	6	$M_{22}^o$	2	2.09	-90	1	-20		-75 1
5	10	27	6	$M_{22}^o$	2.34	2.4	-60	1	-5		-60 1
9	6	13	12	$M_{11}^i$	2.275	2.285	-10	1	20		-35 1
9	6	13	12	$S_{33}^o$	2.01	2.08	-70	1	-10		-65 1
5	7	27	17	$M_{22}^i$	2.14	2.16	-20	1	20		-35 1
5	7	27	17	$M_{22}^i$	2.39	2.48	-90	1	-25		-80 1
5	7	27	17	$S_{55}^o$	2.02	2.07	-50	1	-5		-60 1
5	7	27	17	$S_{66}^o$	2.36	2.42	-60	1	10		-45 1
9	8	21	18	$S_{33}^i$	1.96	2.01	-50	1	-10		-65 1
9	8	21	18	$S_{44}^i$	2.15	2.2	-50	1	5		-50 1
9	8	21	18	$M_{22}^o$	2.01	2.04	-30	1	0		-55 1
9	8	21	18	$M_{22}^o$	2.05	2.08	-30	1	5		-50 1
3	8	16	15	$S_{33}^i$	2.28	2.47	-190	1	-145		-2001

3	8	16	15	$S_{33}^o$	1.68	1.76	-80	1	-10	-65
3	8	16	15	$S_{44}^o$	2.15	2.13	20	1	65	10
2	3	15	11	$M_{11}^i$	2.13	2.08	50	1	90	35
2	3	15	11	$M_{11}^i$	2.34	2.48	-140	1	-70	-125
2	3	15	11	$S_{33}^o$	1.93	2	-70	1	-5	-60
2	3	15	11	$S_{44}^o$	2.45	2.48	-30	1	30	-25
4	9	17	16	$S_{33}^i$	2.11	2.29	-180	1	-130	-185
4	9	17	16	$S_{33}^o$	1.585	1.69	-105	1	-20	-75
4	9	17	16	$S_{44}^o$	2.02	2.03	-10	1	60	5
3	5	23	3	$S_{22}^i$	1.28	1.35	-70	1	-30	-85
3	5	23	3	$S_{33}^o$	1.96	2	-40	1	0	-55
3	5	23	3	$S_{44}^o$	2.02	2.11	-90	1	-45	-100
6	4	22	8	$M_{11}^i$	1.81	1.93	-120	-1	-60	-115
6	4	22	8	$S_{33}^o$	1.76	1.82	-60	-1	-5	-60
2	8	25	2	$S_{33}^i$	2.3	2.41	-110	-1	-60	-115
2	8	25	2	$S_{33}^o$	1.86	1.9	-40	-1	0	-55
2	8	25	2	$S_{44}^o$	1.97	2.02	-50	-1	-5	-60
2	7	18	11	$S_{33}^i$	2.52	2.67	-150	-1	-75	-130
2	7	18	11	$S_{44}^o$	2.21	2.28	-70	-1	-5	-60
7	1	16	14	$S_{33}^i$	2.13	2.26	-130	-1	-60	-115
7	1	16	14	$S_{33}^o$	1.75	1.82	-70	-1	-5	-60
7	1	16	14	$S_{44}^o$	2.07	2.16	-90	-1	-15	-70
1	7	21	6	$M_{11}^i$	1.35	1.48	-130	-1	-35	-90
1	7	21	6	$M_{22}^i$	2.47	2.57	-100	-1	-45	-100
1	7	21	6	$S_{22}^o$	1.31	1.36	-50	-1	0	-55
1	7	21	6	$S_{33}^o$	2.36	2.43	-70	-1	-10	-65
6	9	24	10	$S_{33}^i$	1.92	2.02	-100	-1	-55	-110
6	9	24	10	$S_{44}^i$	2.39	2.58	-190	-1	-140	-195

6	9	24	10	$S_{33}^o$	1.57	1.64	-70	-1	-5	-60
6	9	24	10	$S_{44}^o$	1.76	1.85	-90	-1	-10	-65
2	4	16	11	$S_{22}^i$	1.38	1.46	-80	-1	-5	-60
2	4	16	11	$S_{33}^o$	1.96	2	-40	-1	0	-55
2	4	16	11	$S_{44}^o$	2.24	2.3	-60	-1	-5	-60
8	5	20	14	$S_{33}^i$	1.94	2.03	-90	-1	-25	-80
8	5	20	14	$M_{22}^o$	2.16	2.21	-50	-1	-5	-60
8	5	20	14	$M_{22}^o$	2.25	2.31	-60	-1	-10	-65
2	5	16	12	$S_{22}^i$	1.5	1.57	-70	-1	-25	-80
2	5	16	12	$S_{33}^i$	2.44	2.55	-110	-1	-80	-135
2	5	16	12	$S_{33}^o$	1.84	1.88	-40	-1	0	-55
2	5	16	12	$S_{44}^o$	2.28	2.34	-60	-1	0	-55
5	7	20	12	$S_{33}^i$	2.24	2.38	-140	-1	-90	-145
5	7	20	12	$S_{44}^i$	2.42	2.58	-160	-1	-90	-145
5	7	20	12	$S_{33}^o$	1.67	1.74	-70	-1	-5	-60
5	7	20	12	$S_{44}^o$	1.91	2	-90	-1	-10	-65
1	11	22	9	$M_{11}^i$	1.66	1.77	-110	0	-40	-95
1	11	22	9	$S_{33}^o$	1.58	1.66	-80	0	-5	-60
1	11	22	9	$S_{44}^o$	2.08	2.17	-90	0	-5	-60
1	11	22	9	$S_{55}^o$	2.41	2.58	-170	0	-90	-145
2	12	21	13	$M_{11}^i$	1.54	1.64	-100	0	-55	-110
2	12	21	13	$S_{33}^o$	1.58	1.645	-65	0	-5	-60
2	12	21	13	$S_{44}^o$	1.76	1.91	-150	0	-60	-115
2	12	21	13	$S_{55}^o$	2.6	2.66	-60	0	0	-55
7	7	14	10	$M_{11}^i$	2.42	2.49	-70	0	-15	-70
7	7	14	10	$S_{33}^o$	2.13	2.12	10	0	45	-10
7	7	14	10	$S_{44}^o$	2.56	2.64	-80	0	-5	-60